Broadband Frequency Conversion of Spectrally Incoherent Pulses and Initial Laser-Plasma Instabilities Mitigation Experiments

FINAL REPORT: DE-SC0021032

Christophe Dorrer (co-P.I.), David Turnbull (co-P.I.), Elizabeth Hill (P.M.)

Funded by the DOE Office of Fusion Energy Science

Executive summary

We report on the advances made under the purview of DOE award number DE-SC0021032 that was active during the period: 08/01/2020–07/31/2023. This three-year grant accelerated the development of novel technologies to convert high-energy broadband optical pulses from the infrared to the ultraviolet, and prepared the experimental infrastructure for the first laser-plasma instabilities experiments on the Omega laser facility with the generated pulses having ten times more bandwidth than is currently available.

There is a need for efficient broadband frequency conversion schemes from the infrared, where optical pulses are efficiently amplified by solid-state laser materials, to the ultraviolet, a wavelength range more suitable for inertial confinement fusion (ICF). The current schemes are inadequate for broadband, spectrally incoherent optical pulses composed of a large number of frequency components distributed over a large frequency range. Implementing novel technologies that generate optical pulses with a large number of spectral components improves the laser-target interaction. In particular, it has long been believed that broad bandwidth mitigates the electron-plasma-wave instabilities that generate suprathermal electrons, which degrade ICF performance by increasing the fuel adiabat and reducing the shell areal density. It is important to develop a platform to demonstrate hot electron suppression caused by the larger available bandwidth, which has not previously been feasible in the laboratory. Experimentally measuring and theoretically assessing these effects with adequately benchmarked simulation codes are paramount to the design and development of novel laser facilities aiming at producing energy via laser fusion.

The Laboratory for Laser Energetics is building a new laser facility, the Fourth-generation Laser for Ultrabroadband eXperiments (FLUX), to generate high-energy nanosecond laser pulses with fractional bandwidth larger than 1 % in the ultraviolet and perform combined experiments with the 60-beam Omega facility. This large increase in bandwidth from the ~ 0.1% currently available on high-energy laser systems, is achieved by combining amplification in nonlinear optical parametric amplifiers (OPAs) around 1053 nm (1ω) with nonlinear frequency conversion to the ultraviolet (around 351 nm, 3ω). The novel scheme for frequency conversion is based on the noncollinear sum-frequency generation (SFG) of the angularly dispersed amplified 1ω output with a narrowband 2ω pulse, which is also used to pump the OPA system. The proposal funded scientific and engineering studies necessary to implement this novel laser facility, accelerated the SFG deployment by funding additional project team resources (shop time, engineers, and technicians), and funded preliminary experiments on the Omega Laser.

The personnel supported under this grant were C. Dorrer (co-Principal-Investigator), D. Turnbull (co-Principal-Investigator), E. Hill (Project Manager), as well as engineering resources [Steve Herman (laser engineer), Dave Weiner (Optical Designer), and Dave Nelson (Mechanical Engineer)]. Six peer-reviewed papers have been published in various journals, as listed below. In addition, a patent application, ‘LASER DRIVER MODULE THAT PRODUCES A BEAM OF POLYCHROMATIC DRIVER PULSES USING FEWER PUMP LASERS’ has been filed. The work performed under this grant provided several opportunities for training and professional development, including training of LLE employees on nonlinear frequency conversion, incoherent sources, and broadband optical parametric amplification.

Published peer-reviewed articles:

- C. Dorrer, M. Spilatro, S. Herman, T. Borger, and E. M. Hill, ‘Broadband sum-frequency generation of spectrally incoherent pulses,’ Opt. Express 29, 16135-16152 (2021)
- C. Dorrer and M. Spilatro, ‘Spectral and temporal shaping of spectrally incoherent pulses in the infrared and ultraviolet,’ Opt. Express 30, 4942-4953 (2022).
- C. Dorrer, ‘Analysis of the nonlinear propagation of incoherent pulses,’ Opt. Express 31, 7789-7806 (2023).
- N. Ekanayake, M. Spilatro, A. Bolognesi, S. Herman, S. Sampat, E. M. Hill, and C. Dorrer, ‘Design and optimization of a high-energy optical parametric amplifier for broadband, spectrally incoherent pulses,’ Opt. Express 31, 17848-17860 (2023).

- D. Turnbull, J. Katz, D. E. Hinkel, P. Michel, T. Chapman, L. Divol, E. Kur, S. MacLaren, A. L. Milder, M. Rosen, A. Shvydky, G. B. Zimmerman, and D. H. Froula, 'Beam Spray Thresholds in ICF-Relevant Plasmas,' Phys. Rev. Lett. 129, 025001
- D. Turnbull, J. Katz, T. Chapman, J. Ludwig, P. Michel, and D. H. Froula, 'Smoothing by Spectral Dispersion Can Exacerbate Beam Spray' in preparation for Physics of Plasmas

I. MOTIVATION

The effective laser energy available for laser-driven inertial confinement fusion interactions and many other high-energy laser–target interactions is predominantly limited by laser–plasma instabilities (LPI's) such as cross-energy beam transfer (CBET), stimulated Raman scattering (SRS), and two-plasmon decay (TPD). Recent theoretical studies have shown that drive lasers with sufficiently broad spectral bandwidths exceeding 1% ($\Delta\omega/\omega > 1\%$) would mitigate such adverse effects occurring in intense laser–target interactions by increasing the fraction of laser photons absorbed by the target through hindering the coherent instabilities, hence significantly increasing both ongoing and future experimental capabilities [1-5].

The current generation of large-scale, high-energy solid-state laser systems capable of delivering kilojoule-level single laser pulses is based on Nd:glass amplifiers operating around the near-infrared wavelength of 1053 nm (1ω) and frequency tripling to 351 nm (3ω) using large-aperture nonlinear crystals. Due to the spectral gain narrowing occurring in Nd:glass amplifiers and the limited spectral acceptance of the tripling process, however, the typical fractional spectral bandwidth delivered by these high-energy lasers is typically limited to $\Delta\omega/\omega < 0.1\%$ [6-8]. Such fractional bandwidth is insufficient to significantly mitigate LPI.

The Fourth-generation Laser for Ultrabroadband eXperiments (FLUX) is currently being developed at the Laboratory for Laser Energetics to meet the demand for broad spectral bandwidths. FLUX relies on optical parametric amplification and sum-frequency generation (SFG) to deliver spectrally incoherent pulses with a fractional spectral bandwidth exceeding 1% in the UV (351 nm) [Fig. 1(a)]. In contrast to laser amplifiers, FLUX utilizes optical parametric amplifiers (OPA's) that offer a pathway to achieve the required fractional bandwidth because optical parametric amplification can be phase matched to amplify spectrally incoherent broadband pulses [9-11]. In addition, a novel angularly dispersed noncollinear geometry for broadband frequency conversion via SFG of broadband 1ω pulses and narrowband 2ω pulses [12], as described in the next section of this report, will be implemented in FLUX to achieve the intended fractional spectral bandwidth of 1.5%. FLUX will produce on-target radiation that is analogous to the StarDriver™ concept [13], where a large number of uncorrelated relatively narrowband laser sources operating at different wavelengths are used to compress an ICF target [Fig. 1(b)]. The increased bandwidth suppresses the growth of laser-plasma instabilities (LPI), resulting in higher absorption than currently obtained with low-bandwidth pulses (fractional bandwidth of the order of 0.1%), while simultaneously mitigating hot electron generation produced by electron plasma wave (EPW) instabilities. Higher bandwidth is expected to decrease the beam imprint and reach the smoothing asymptotic limit much faster than on current laser systems, resulting in reduced hydrodynamic instabilities, which will improve the efficiency and stability from better target compression.

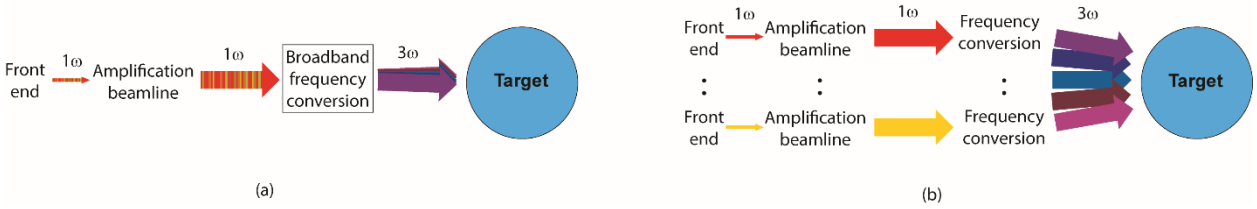

Fig. 1. Concept for (a) FLUX, based on a single broadband spectrally incoherent beam generated in a single beamline, with novel broadband frequency-conversion scheme, and (b) StarDriver™, based on uncorrelated narrowband beams at different wavelengths independently generated, amplified and frequency converted.

Developing a prototype StarDriver™ system to demonstrate the advantages of this concept would require the implementation of a large number (thousands) of seed sources and amplifiers. It is neither economically nor technically practical to build a low-energy prototype that would support initial studies of physical processes and optimization of the system's parameters toward the construction of an ICF-scale StarDriver™ system. Instead, the developed frequency-conversion technology employs a novel combination of many of the components already developed for ICF systems, e.g., nonlinear crystals and

diffraction gratings used on the National Ignition Facility at the Lawrence Livermore National Laboratory (LLNL) [7] and the Laser MegaJoule at the Commissariat à l'Energie Atomique [14]. It will enable a significant step toward the understanding of laser-matter interaction at ICF-relevant intensities with spectrally incoherent pulses and allow for important technological developments in solid-state laser technology.

To test the LPI mitigation predictions and demonstrate the required laser bandwidth to eliminate laser-plasma instabilities in ignition-relevant fusion plasmas, new LPI platforms were proposed for OMEGA, building on the recent successes of the CBET Platform [15]. By using similar underdense gas-jet targets preheated by ~10 low-intensity heater beams and characterized using Thomson scattering [16], we aim to study the impact of bandwidth on filamentation as well as backscatter instabilities in conditions resembling the high-gain regions in NIF hohlraums. Solid-target platforms (either planar, spherical, or conical) recreate the coronal plasma conditions of a directly driven implosion and will allow us to study the effects of bandwidth on the TPD and SRS instabilities, which pose a major preheat risk. Likewise, the flowing plasmas surrounding driven spherical targets can be used to examine the influence of bandwidth on CBET in implosions. Our goal during this grant was to begin developing these platforms using a narrowband 3ω beam injected into the same P9 port to which FLUX will ultimately be directed.

II. PROGRESS UNDER THIS GRANT

This grant funded scientific and engineering studies related to the FLUX system, in particular, the generation and propagation of high-energy incoherent pulses, as well as their transport and on-target focusing. These studies accelerated the design and deployment of the FLUX SFG stage. The modeling and analysis tools that have been developed will support the deployment and operation of FLUX, and will play a role in the design of future broadband laser systems. The grant also funded three shot days to develop various experimental LPI platforms on the OMEGA-60 Laser Facility. The progress in these areas is described in the following sub-sections.

II.1. Sum-frequency generation of broadband incoherent pulses

This grant supported the analysis and design of a broadband sum-frequency-generation stage to frequency convert incoherent pulses from 1ω to 3ω. This stage is necessary to frequency convert the broadband output pulse from FLUX's main amplifier, spectrally centered at 1053 nm, to a broadband pulse centered at 351 nm. More generally, such frequency-conversion approach could be beneficial to future laser facilities.

On high-energy solid-state laser facilities, the amplified output pulse at 1ω must be converted to 3ω for more favorable interaction conditions. The standard tripling schemes rely on two nonlinear crystals, a doubler that converts a fraction of the incoming 1ω pulse into a 2ω pulse, and a tripler that mixes the generated 2ω pulse with the remaining 1ω pulse, resulting in a 3ω pulse [Fig. 2(a)][17]. Such scheme does not allow for frequency conversion of a broadband 1ω pulse. A related scheme uses angular dispersion introduced by a diffraction grating to better match the propagation direction of the different frequency components of the pulse to the phase-matching conditions in the nonlinear crystal [Fig. 2(b)][18]. A specific value of the angular dispersion leads to broadband frequency conversion for a phase-modulated pulses, but this approach is inefficient for incoherent pulses.

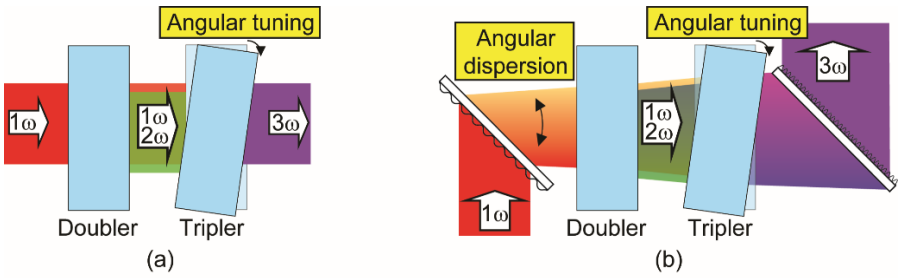

Fig. 2. Third-harmonic generation with doubler and tripler (a) without and (b) with angular dispersion, with degrees of freedom for operation highlighted in yellow.

The sum-frequency-generation stage of the FLUX system relies on the interaction of the broadband 1ω pulse with a narrowband 2ω pulse (Fig. 3)[12]. This interaction is not collinear, i.e., a small angle is introduced between the two beams. Angular dispersion is added on the 1ω beam by a diffraction grating. The nonlinear interaction between the 1ω and 2ω pulses generates a 3ω pulse. The work supported by this grant established the conditions for which this nonlinear interaction can be phase-matched over a large range of 1ω frequencies to efficiently frequency convert the broadband 1ω FLUX pulse into a broadband 3ω pulse. This was achieved by developing analytical solutions to the phase-matching configuration being considered and computer code that simulates the nonlinear interaction. Additionally, a laser test bed was developed to study this novel frequency-conversion geometry as a function of its three degrees of freedom and demonstrate, at a small scale, the broadband frequency conversion of incoherent pulses from 1ω to 3ω.

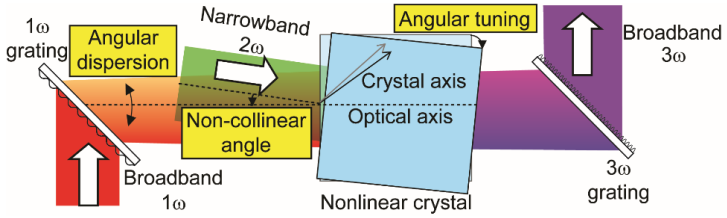

Fig. 3. Broadband sum-frequency generation from 1ω to 3ω, suitable to generate spectrally incoherent pulses with fractional bandwidth larger than 1%. The three degrees of freedom in this scheme are the angular dispersion on the 1ω beam, the non-collinear angle between the 1ω and 2ω beam, and the crystal tuning angle.

The three-wave nonlinear mixing interaction has been modeled as a function of the wavevectors of the waves at 1ω, 2ω, and 3ω (Fig. 4). The resulting wavevector mismatch Δk is a function of the crystal angle θ, the noncollinear angle α between 1ω and 2ω waves, the resulting angle Ω between the 1ω and 3ω waves, and the angular dispersion coefficient D. Δk can be developed as a function of the frequency ω relative to the central frequency in the 1ω pulse. An efficient nonlinear interaction requires that the wavevector mismatch be 0. For broadband frequency mixing, it is therefore necessary that the linear dependence of Δk with respect to ω be 0. This sets the analytical relation between the noncollinear angle and the angular dispersion. This analysis is in excellent agreement with a computational model that determines the wavevector mismatch (Fig. 5). The results show that a continuum of solutions exist for broadband frequency conversion, i.e., the non-collinear angle can be chosen for a given angular dispersion. This is beneficial to the implementation of the FLUX system because it allows for the use of a grating technology already developed for high-energy laser systems at 1ω and 3ω, namely frequency conversion on the CEA Laser MegaJoule. Based on this study, the line spacing for the 1ω and 3ω diffraction gratings is approximately 800 l/mm and 2400 l/mm for the FLUX test-bed (described in the next paragraph) and the FLUX system.

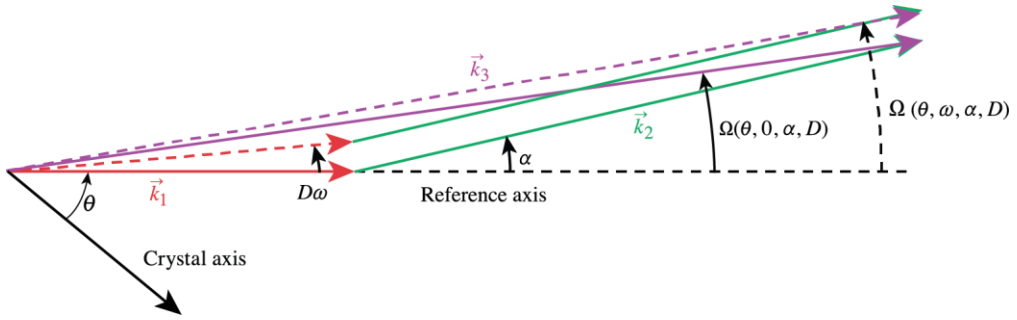

Fig. 4. Configuration for the noncollinear sum-frequency generation of an angularly dispersed broadband 1ω wave (red wave vectors) with a narrowband 2ω wave (green wave vector), yielding a broadband angularly dispersed 3ω wave (purple wave vectors). The wave vectors at ω = 0 and at a sample ω ≠ 0 are displayed with a continuous line and a dashed line, respectively.

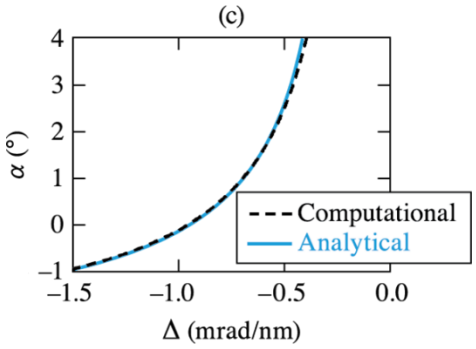

Fig. 5 Relation between noncollinear angle a and angular dispersion D for broadband frequency conversion, determined computationally (dashed black line) and analytically (solid blue line).

This grant supported the development of a testbed to check this novel SFG scheme as well as personnel for operation. A schematic of the test bed is presented in Fig. 6. The testbed uses a fiber front end and amplifiers to generate a broadband incoherent pulse. The sum-frequency-generation has the same functionality as drawn on Fig. 3, but image relays have been introduced between the 1ω grating and the SFG crystal, and between the SFG crystal and the 3ω grating because of the small beam size (~ 1 mm). All details of the test-bed can be found in a peer-reviewed publication [12]. The test-bed was also used to investigate techniques to spectrally and temporally shape incoherent pulses [19], and is now used for damage testing of optical components with incoherent pulses.

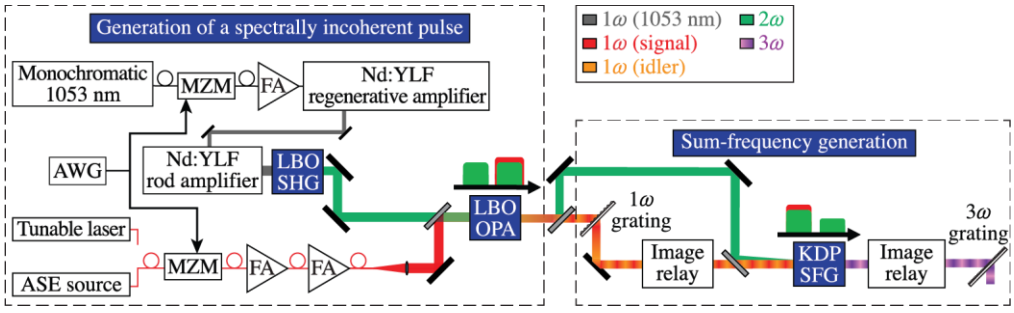

Fig. 6. Experimental layout for generation of a broadband spectrally incoherent pulse (left-hand side) and sum-frequency generation (right-hand side).

The non-collinear angle was first optimized for the angular dispersion induced by the 1ω grating. The phase-matching properties of the SFG stage were then investigated as a function of wavelength and angular detuning of the nonlinear crystal (Fig. 7). At the optimal angle (δθ = 0), a large range of wavelengths around 1053 nm can be frequency converted to 3ω. With angular detuning of the crystal (δθ > 0), this range

splits into two components that are symmetric relative to the central 1ω wavelength (1053 nm). Such configuration is advantageous for the FLUX system because the signal and idler coming from the high-energy collinear parametric amplifier are symmetric in frequency relative to 1053 nm. This combination of signal and idler leads to a large fractional bandwidth. Broadband operation of the SFG stage was confirmed by measuring its output vs tuning angle for an input broadband incoherent pulse. This input pulse is the combination of the signal and idler from the previous optical parametric amplifier, and its spectrum is therefore representative of the last output of the FLUX main amplifier. As shown on Fig. 8, the resulting 3ω pulse is broadband, covering more than 10 THz of bandwidth. Based on these experimental and modeling results, a large KDP crystal with 10-mm thickness and 15×15 cm^2 aperture has been procured for FLUX.

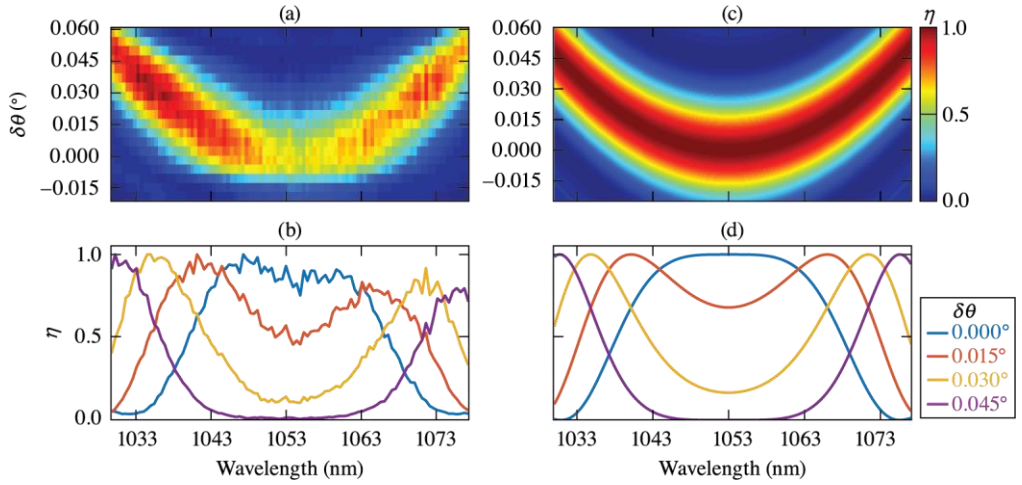

Fig. 7. SFG efficiency in the broadband configuration for a 10-mm KDP crystal as a function of 1ω wavelength and crystal angle, measured on the FLUX test-bed [(a), (b)], and modeled [(c), (d)].

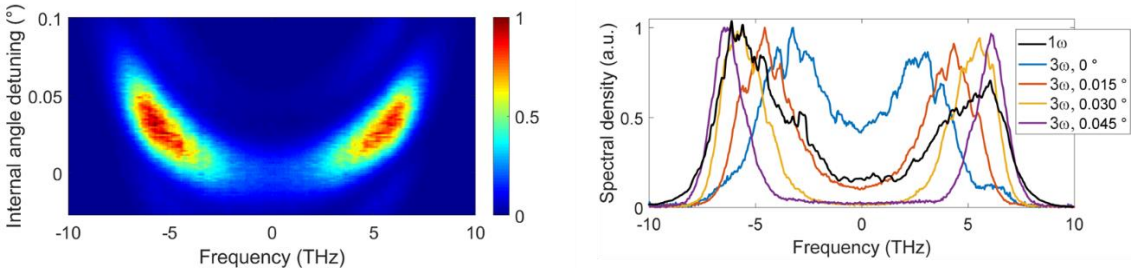

Fig. 8. SFG of a spectrally incoherent source for various crystal detunings relative to phase matching at 1053 nm, for a 10-mm KDP crystal. On (b), the spectral density of the 1ω wave as a function of the frequency detuning relative to its central frequency (upper horizontal axis) is indicated with a black line.

II.2. Achromatic transport and focusing of broadband 3ω pulses

The large bandwidth of the optical pulses at 3ω that will be generated by the FLUX system makes them particularly susceptible to the chromatic dispersion of glasses that compose the optical components commonly used on laser systems. The chromatic dispersion of an optical glass impacts refraction at its interface with another medium (typically air), leading to angular dispersion (wavelength-dependent propagation direction). The two main areas of concern that were addressed during this grant are angular dispersion caused by optical wedges in the beam path from the SFG stage to the Omega Target Bay, and chromatic aberrations of the upcollimator and Omega focusing lens. In each case, optical models have been developed to quantify the impact of various technical choices on performance (e.g., the resulting on-target focal spot), and an optimal solution has been chosen. The following two sub-sections describe the issues to be addressed and the solutions that are being implemented on the FLUX system.

Angular dispersion from wedges

Refraction at the interface between two media of index n_1 and n_2 at the wavelength λ leads to the relation $n_1(\lambda)\sin[\theta_1(\lambda)] = n_2(\lambda_2)\sin[\theta_2(\lambda)]$ linking the propagation angles θ_1 and θ_2 relative to the surface normal. Propagation through a wedged component such as a wedge used as a pick-off for a low-energy sample of the main beam sent to a diagnostic leads to a wavelength-dependent propagation direction on the main beam going through it, i.e., a linear transverse spread in the far field. This angular dispersion therefore elongates the focal spot, potentially lowering the on-target intensity.

The FLUX beam path from the SFG output to the Omega focusing lens nominally includes two wedged optics: the wedge for the 3ω diagnostic suite at the output of the FLUX system (fused silica, angle = 0.5°, in the 12-cm beam space after the FLUX SFG stage) and the Omega Full-Aperture Back-Scatter (FABS) diagnostic (fused silica, angle = 1°, in the 29-cm beam space after the FLUX upcollimator), as shown on Fig. 9. It was determined that these two wedges, which introduce angular dispersions of different magnitude in different directions, cannot compensate for each other and would result in an unacceptable elongation of the on-target focal spot. A flexible engineering solution based on two wedged fused-silica windows in the FLUX beam path has been developed. These windows are required to isolate physical spaces having different cleanliness requirements, and manufacturing/installing wedged windows, instead of parallel windows, is not a significant additional cost to the project.

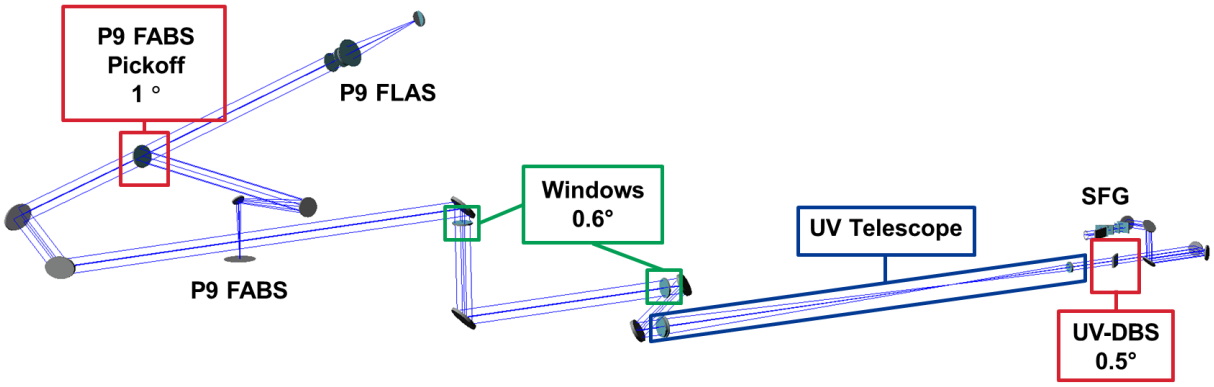

Fig. 9. Optical layout of the 3ω beam transport from the SFG stage to the Omega focusing lens assembly (P9 FLAS). The two diagnostic wedges are identified by red boxes. The UV telescope upcollimating the beam from a 12-cm diameter (output of SFG stage) to a 29-cm diameter (full Omega beam size) is identified by a blue box. The two wedged windows added to compensate the residual angular dispersion are identified by green boxes.

Analytical calculations and ray-tracing determined that the compensation of residual angular dispersion in the target plane can generally be achieved as long as the wedge angle of the two additional windows (which are identical, for the sake of manufacturing cost) is large enough. The lowest acceptable wedge angle, ~0.46°, leads to good compensation, as shown by the absence of significant displacement of rays at different wavelengths around 351 nm (Fig. 10). Such theoretical solution, however, does not consider the practical uncertainties in characteristics and alignment of all components in the beam path. Wedged windows with a larger wedge angle offer additional flexibility: their relative orientation can be adjusted to compensate a range of angular dispersions around the modeled value, instead of a single angular dispersion. For larger wedge angles, there are generally two sets of windows orientations that can compensate the overall angular dispersion. A wedge angle equal to 0.6° was chosen, leading to excellent compensation of the residual angular dispersion (Fig. 11). Ray-tracing was used to confirm that implementing these wedged windows does not lead to beam clipping on the mirrors, A flexible mounting scheme allowing for precisely setting the orientation of these two windows has been designed. The wedged windows and mechanical mounts are in the process of being manufactured.

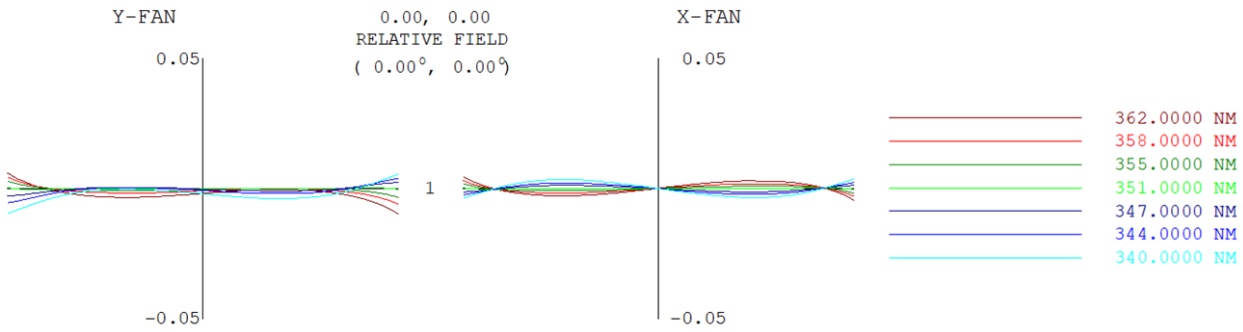

Fig. 10. Ray aberrations (in mm) at the Omega target plane as a function of wavelength (from 340 nm to 362 nm) for the optimal orientation of the two windows with wedge angle = 0.456 °.

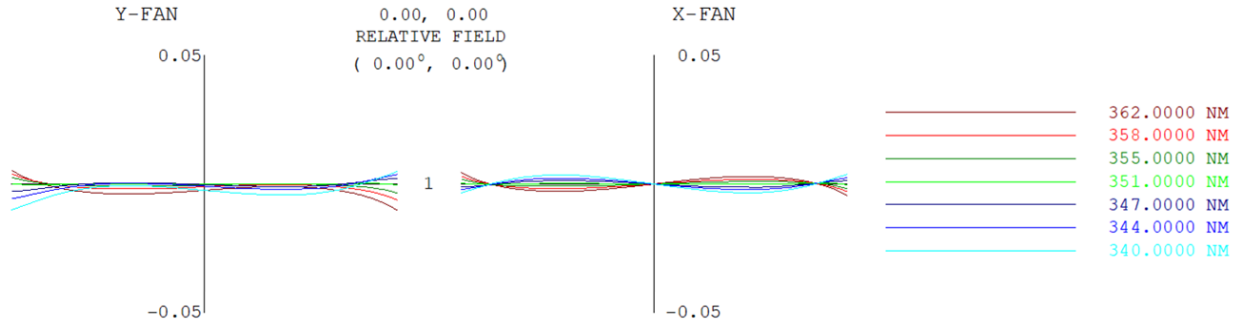

Fig. 11. Ray aberrations (in mm) at the Omega target plane as a function of wavelength (from 340 nm to 362 nm) for the optimal orientation of the two windows with wedge angle = 0. 6 °.

Achromatic focusing of broadband UV pulses

The focusing of the FLUX beam will be performed through port P9 with the existing focus lens (Fig. 9). This fused-silica lens is suitable for narrowband 3ω pulses, but its chromatic aberrations are too large for the broadband FLUX pulses. These aberrations lead to a wavelength-dependent focal length, which would result in a wavelength-dependent focal spot on target. This has for effect to distort the focal spot obtained with a phase plate, reduce the on-target intensity, and modify the spectral content at different points in the target plane, hence these aberrations could significantly impact the laser-matter interactions. An example is shown in Fig. 12(a), which represents the modeled focal distribution of rays at the FLUX central wavelength (351 nm, green dots) and two extreme wavelengths (347 and 355 nm, blue and red dots) resulting from focusing of an ideal beam by the standard fused-silica Omega focus lens. The focal spots at the two extreme wavelengths are approximately 400-μm in diameter, which is not acceptable considering the FLUX focal-spot and intensity requirements, which are based on using an SG4 phase plate resulting in a 100-μm focal spot. Furthermore, an optical telescope in the transport system is required to increase the size of the FLUX beam from ~ 12 cm (at the SFG stage) to ~ 29 cm (standard Omega beam size). Such telescope, if implemented with fused-silica lenses, would further increase the chromatic aberrations and reduce the achievable on-target intensity.

As a result of various design studies, it was decided to keep the existing fused-silica focusing lens and implement an upcollimating telescope that compensates its own chromatic aberrations and precompensates the aberrations of the focus lens. Such telescope is a combination of four lenses made of different glasses. The glasses were chosen based on UV transmission, relatively low nonlinear coefficient, and optical performance. The resulting spot diagram is shown in Fig. 12(b). An essentially diffraction

limited performance is obtained over the FLUX bandwidth, which is important to meet the FLUX on-target intensity requirements. The designed lens assemblies are currently being manufactured.

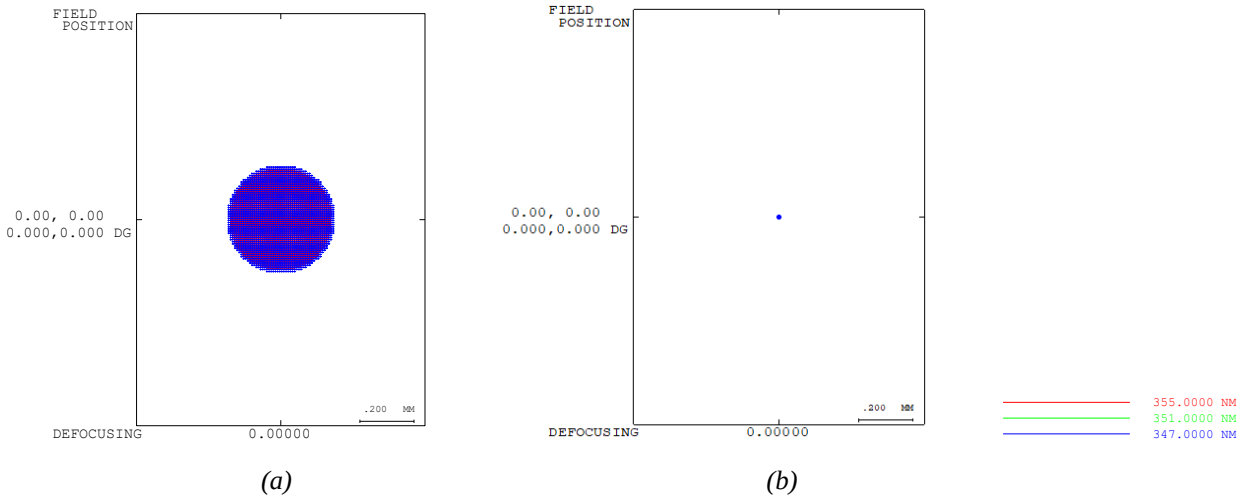

(a) *(b)*

Fig. 12. Modeled spot diagram at three wavelengths considering (a) focusing of an ideal beam by the Omega fused-silica focusing lens and (b) an upcollimation telescope composed of four lenses of different glasses followed by the Omega fused-silica focusing lens.

II.3. Propagation of broadband incoherent pulses

The lack of coherence between the spectral components of FLUX pulses leads to highly modulated temporal profile (the temporal equivalent of a spatial speckle field) [Fig. 13(a)]. This field is characterized by its coherence time (the inverse of the overall bandwidth) and the probability density function (PDF) of the instantaneous power. The power PDF of a field with uncorrelated spectral components is a negative exponential, indicating that the power can, in theory, have arbitrary high values [Fig. 13(b)]. In practice, the PDF is modified by processes such as amplification and frequency conversion. The high values of the power relative to its average value enhance nonlinear processes, which is a particular concern for self-phase modulation (SPM). SPM induces a temporal phase that is proportional to the intensity (a function of time and the transverse coordinates). In a medium with a positive nonlinear index n_2, e.g., all the glasses and crystals commonly used in high-energy laser systems, SPM can lead to small-scale self-focusing. This self-focusing process, which is seeded by intrinsic modulation of the beam amplitude, increases the local intensity of the beam. The local increase can be sufficient to cause optical damage in the component in which it occurs or in down-stream components.

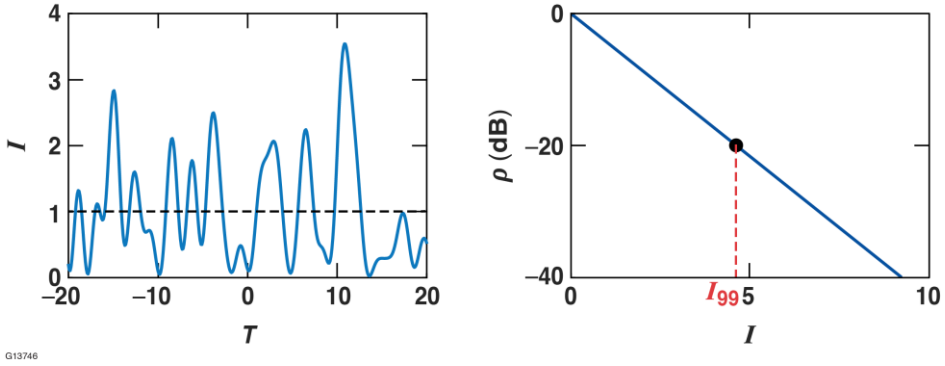

Fig. 13. (a) Example of temporal profile of an incoherent pulse with normalized coherence time equal to 1 (note the large random modulation with spikes having a typical duration of the order of 1). (b) Probability density function of the intensity (blue line), with the expected analytical PDF (dashed black line). The black marker indicates I_{99}, the 99th percentile of the intensity PDF I_{99} (intensity for which 99% of the intensity values within the pulse are between 0 and I_{99}).

A statistical model has been developed to understand the nonlinear propagation of incoherent pulses [20]. This analysis has been performed in two different frameworks. First, the nonlinear propagation was studied purely in the time domain to understand the interplay between nonlinear propagation and chromatic dispersion within the medium. The study was then extended to one spatial coordinate, following the Bespalov-Talanov framework that is commonly applied to nanosecond coherent pulses [21]. The statistical properties of the pulse after propagation were quantified by its PDF, the stretching exponent which qualifies the shape of the PDF and its behavior at high intensity values, the scintillation noise (rms variation of the intensity), and the 99th percentile of the intensity PDF I_{99} (intensity for which 99% of the intensity values within the pulse are between 0 and I_{99}). Statistically relevant PDFs were generated using a large number of simulation runs performed for different initial random fields. The nonlinear medium was characterized by its nonlinearity, quantified by the total nonlinear phase accumulated by a pulse of normalized average intensity equal to 1, and its chromatic dispersion, used to normalize the coherence time of the pulse.

The time-domain simulations show that the sign of the chromatic dispersion plays an important role in the statistical properties of the output pulse (Fig. 14). The intensity PDFs of the incoherent pulse is not significantly modified for broadband pulses ($\Delta T<<1$), with a pulse shape that changes significantly during dispersive propagation in the medium, and narrowband pulses ($\Delta T>>1$), with a pulse shape that remains identical during propagation. For intermediate coherence time, a medium with positive φ_2 can lead to a reduction of the likelihood of getting high intensity values. In this case, nonlinear dispersive propagation clamps the intensity profile, essentially decreasing the intensity of the random intensity spikes. The materials commonly used in high-energy lasers, including the fibers used in the front end, have a positive dispersion at 1053 nm and 351 nm. In a medium with a negative φ_2, an increase in the likelihood of getting high intensity values is observed. In such medium, nonlinear dispersive propagation enhances the intensity of the random intensity spikes. Such behavior could for example be observed in optical fibers at 1550 nm, for which the combination of material's dispersion and waveguide dispersion leads to a residual negative dispersion.

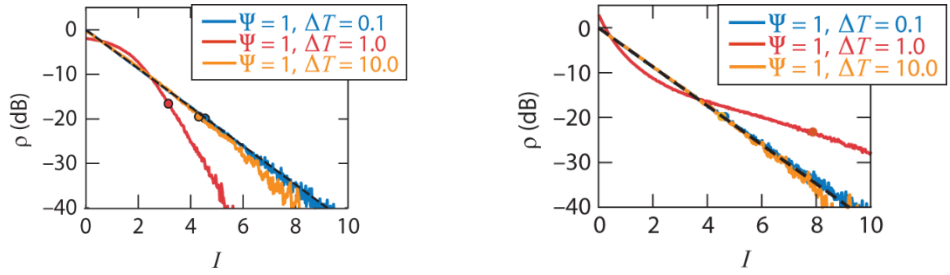

Fig. 14. Intensity PDF for nonlinear propagation in a medium with (a) positive and (b) negative dispersion. These results correspond to the same average nonlinear phase $\psi = 1$ rad and different coherence time ranging from $\Delta T = 0.1$ (broadband) to $\Delta T = 10$ (narrowband).

Adding a spatial coordinate introduces an interplay between temporal modulation and spatial modulation. In the Bespalov-Talanov framework, a sinusoidal modulation is introduced on the spatial profile, and its amplitude increases via nonlinear propagation in a common medium with positive n_2. This amplitude increase corresponds to small-scale self-focusing around maxima of the modulation. In a dispersive medium with positive dispersion φ_2, this amplitude increase in the spatial domain can be mitigated by the decrease occurring in the temporal domain. This leads to a complex interplay between the temporal and spatial effects, which leads to mitigation of self-focusing in some propagation regimes [20].

II.4. Experimental platform development

The first shot day reserved for FLUX platform development—SRSPlatform-21C—was completed in August 2021. While the campaign name implies a focus on platform development specifically to look at stimulated Raman scattering (SRS), we have broadened the goals to look at a wider range of laser-plasma

instabilities including stimulated Brillouin scattering (SBS) and beam spray ("filamentation") in addition to SRS. We anticipate that it will be more impactful to demonstrate that bandwidth mitigates *all* laser-plasma instabilities that have plagued inertial confinement fusion research for decades.

This initial shot day focused on generating those instabilities using narrowband 3ω light in our gas jet target platform. The gas jet provides homogenous, ~mm-length-scale plasmas that allow for convective instability gains to be quite large when the interaction beam is tightly focused to high intensity (~10^{15} W/cm^2). The goal was to identify appropriate regions in parameter space where each instability can be studied in isolation. SBS is preferentially driven when electron-plasma-wave damping is large but ion-acoustic-wave damping is small, which are both more likely in a mid- to high-Z plasma, and so we used pure nitrogen gas at an intermediate density to promote SBS backscatter. Conversely, SRS is driven when electron-plasma-wave damping is weak but ion-acoustic-wave damping is strong, which is more likely in low-Z plasmas at higher density, so we used methane gas at intermediate and high density to promote SRS backscatter. And finally, beam spray can be isolated when the intensity is high but both electron-plasma-wave and ion-acoustic-wave damping are also strong, so lower-density methane was also studied to access this regime.

An interaction-beam intensity scan was performed in each parameter space. In higher-density methane [Fig. 15(b)], as expected SRS backscatter ramped up and the transmission dropped precipitously (which is reminiscent of low-gas-fill NIF indirect-drive hohlraums). Conversely, SBS backscatter dominated the results in the pure-nitrogen plasma [Fig. 15(a)], with reflectivity approaching 40% at the highest intensity.

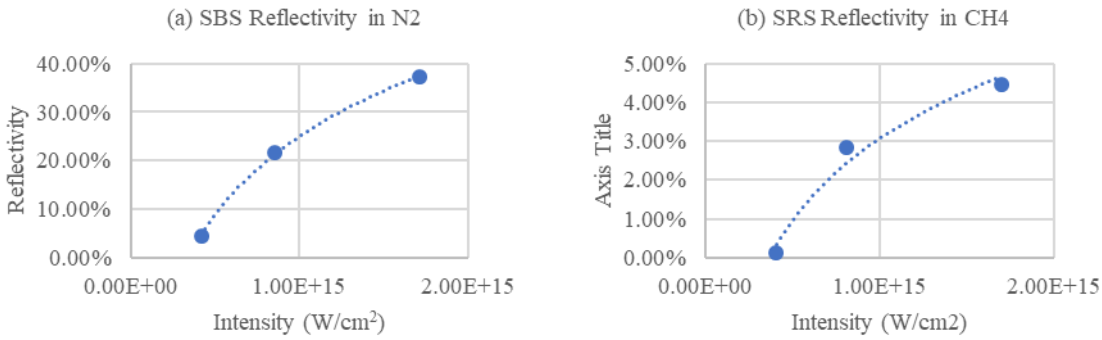

Fig. 15. (a) SBS backscatter was very large in nitrogen plasmas with weak ion-acoustic wave damping. (b) SRS backscatter dominated when ion-acoustic wave damping was larger but electron-plasma wave damping was weaker in higher-density C-H plasmas.

The main goal of this experiment was to develop platforms and perform experiments that can be repeated in the future with FLUX to demonstrate that bandwidth mitigates the instabilities. However, the narrowband results were already of interest in isolation since LPI experiments have not typically been conducted as systematically or diagnosed as rigorously. Beam spray in particular was a source of much discussion during the 2020 ICF workshop within the hohlraum physics working group, which suggested that it was potentially interesting to revisit this topic. While the onset of beam spray was captured in the absence of any backscatter in low-density methane, it was less straightforward to isolate the backscatter instabilities from beam spray, and in fact all of the results were affected by beam spray to some degree. We have a unique ability to diagnose beam spray quantitatively because the P9 transmitted beam diagnostic collection is f/4 whereas the incident beam is f/6.7, enabling full accounting of the transmitted beam even in the event of significant spray (Fig. 16). Also, the transmitted beam power is measured with a streaked spectrometer, and the spectral shifts that were observed provided a clear signature for the relevant mechanism involved in the beam spray.

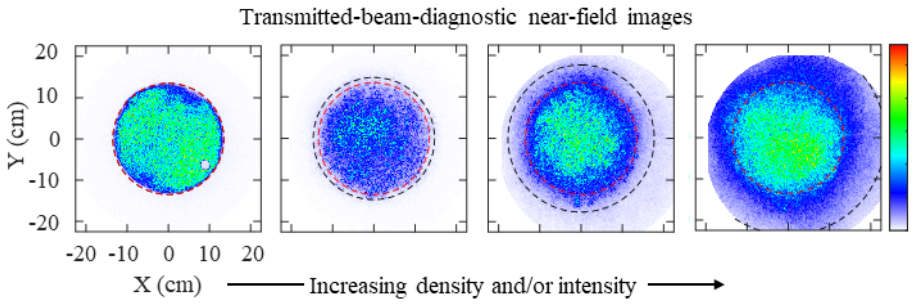

Fig. 16. Examples showing the increasing amount of beam spray that was observed with increasing density and laser intensity.

It turns out that beam spray at moderate intensity is caused strictly by small-angle forward SBS (FSBS), making "filamentation" a misnomer, and the "filamentation figure of merit" that is frequently used to predict the onset of beam spray can overestimate the threshold by more than an order of magnitude. A recent theory paper [22] predicted lower thresholds for FSBS and also suggested there should be a dependence on ion-acoustic-wave damping. Our experiments confirmed both these predictions and showed that the onset of beam spray coincided in each case much more closely with their revised "Grech" Figure of Merit, as shown in Fig. 17 [23].

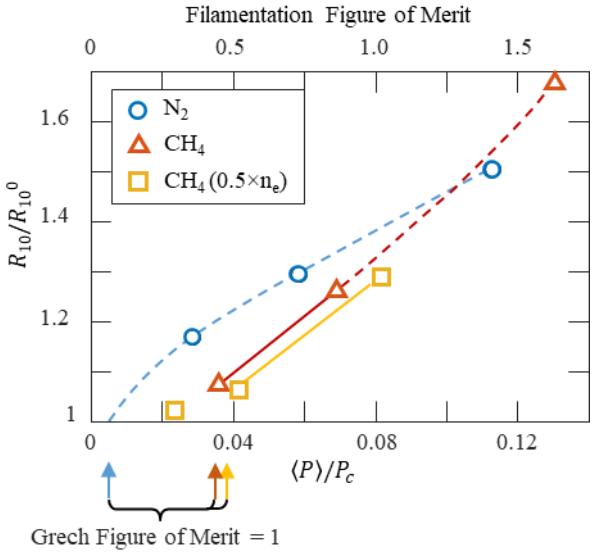

Fig. 17. The onset of beam spray in each data set was found to occur at intensities below the widely used "Filamentation Figure of Merit," and appeared much more consistent with the "Grech Figure of Merit," validating its additional terms.

The second shot day featured solid targets—both typical planar targets as well as novel cone-shaped targets that generate coronal plasmas with longer density scale lengths than is traditionally possible on OMEGA—in order to develop a platform that can be used to study direct-drive ignition-scale TPD and SRS. The coronal plasmas were preformed by 9 beams arranged in two cones for 1 ns. Those beams were then turned off and the P9 interaction beam turned on to study the instabilities driven by that beam in isolation. An example of the results is shown in Fig. 18. Backscatter from the interaction beam was spatially, temporally, and spectrally resolved using a new P9 full-aperture backscatter (FABS) diagnostic built for this purpose. Half-harmonic emission from the TPD instability was also expected in the spectral data along this line of sight. Raman sidescatter was also observed in both the B30 FABS (with temporal and spectral resolution) and a scattered-light uniformity imager (SLUI) in TIM4 (with spatial resolution).

We observed a prevalence of both Raman backscatter and sidescatter from relatively low densities and no evidence of the TPD or absolute SRS instabilities that are typically active at the quarter-critical density in OMEGA implosions. It turns out that Raman backscatter and sidescatter are both much more common in high-intensity single-beam experiments like this one, but are less often observed in multibeam configurations. In single-beam experiments, Raman backscatter is often observed below the expected threshold based on convective gains in inhomogenous plasmas, and this is usually attributed to filamentation producing regions of higher intensity than would normally be present. Raman sidescatter, on the other hand, is less prevalent in multi-beam experiments because it is more difficult to satisfy a common-wave configuration for sidescatter that it is for TPD, for example. The lack of evidence for TPD is not entirely understood—the competing instabilities may reduce the laser's power and coherence in such a way that it can no longer drive instability at the quarter-critical density, but the P9 backscatter diagnostic may also need greater sensitivity to half-harmonic emission (this will be improved in the future).

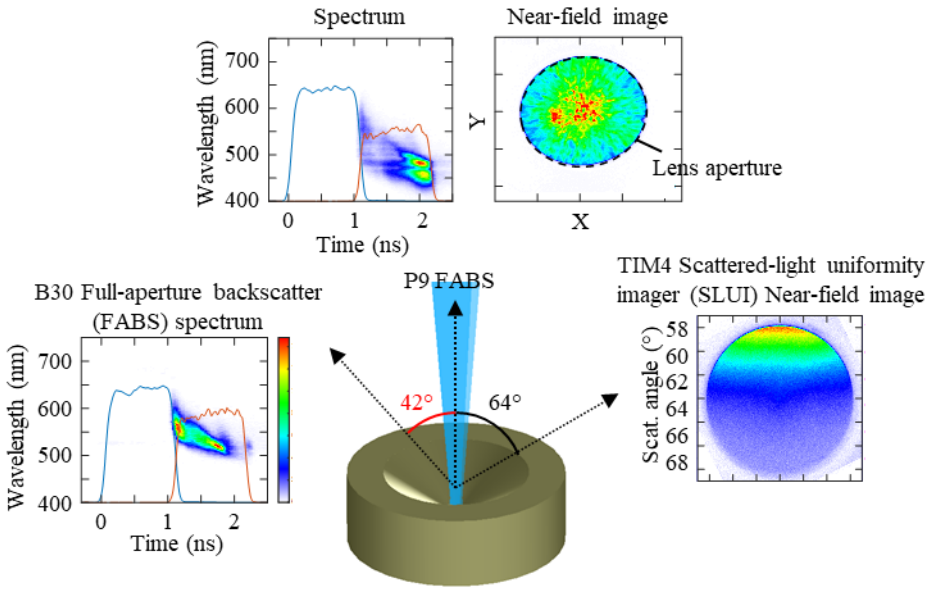

Fig. 18. During the interaction beam, sidescatter and backscatter were diagnosed using the P9 FABS diagnostic, B30 FABS, and a TIM-based SLUI detector.

However, given the prominence of TPD in direct-drive implosions at current OMEGA-scale, it is of great interest to be able to study TPD using FLUX. The most salient difference between traditional single-beam and multi-beam irradiation is simply the effective f-number, where a single OMEGA beam is typically focused at f/6.7 while a multi-beam unit (either a pent of hex of beams) is at most ~f/1. This changes the speckle size dramatically (Fig. 19) and in turn the nature of the instabilities that are driven in the radiation field.

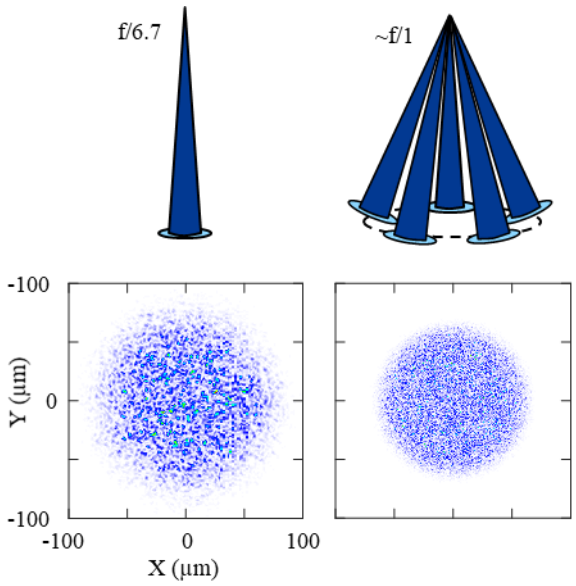

Fig. 19. Speckle pattern of an f/6.7 beam compared to an f/1 beam

As a result, f/1 focusing capability has been added as a requirement for the fielding of FLUX. This is being actively worked on at the moment, and our expectation is that the capability will be available starting in FY'25 for the second year of shots with FLUX. We should then be able to repeat similar experiments but observe a prominence of TPD more reminiscent of current direct-drive implosions when driven by a narrowband beam. Using FLUX, we expect to observe higher thresholds and reduced instability levels, and if so it will be one of the most impactful results we can deliver.

Our final platform-development shot day was split into two half-day campaigns. The goal of the first campaign was to acquire backscatter and filamentation data with an intermediate level of bandwidth in between the no-bandwidth results from the first shot day (Figs. 15 and 17) and FLUX-level bandwidth in the future. Four shots were executed to interpolate between results in two of the previous data sets. Our motivation is to be able to show much more dramatic effects on LPI using FLUX compared to the current state-of-the-art using either the smoothing-by-spectral-dispersion (SSD) or induced-spatial-incoherence (ISI) techniques. This will allow us to contrast our results from papers in the early '90s that showed sometimes dramatic effects on certain instabilities just with the addition of ISI-level bandwidth. OMEGA's 2-D SSD system was fielded at roughly half its full bandwidth capability in order to reduce the coherence time to ~6 ps while minimizing the change to the far-field spatial profile for ease of comparison to the earlier experiments (Fig. 20).

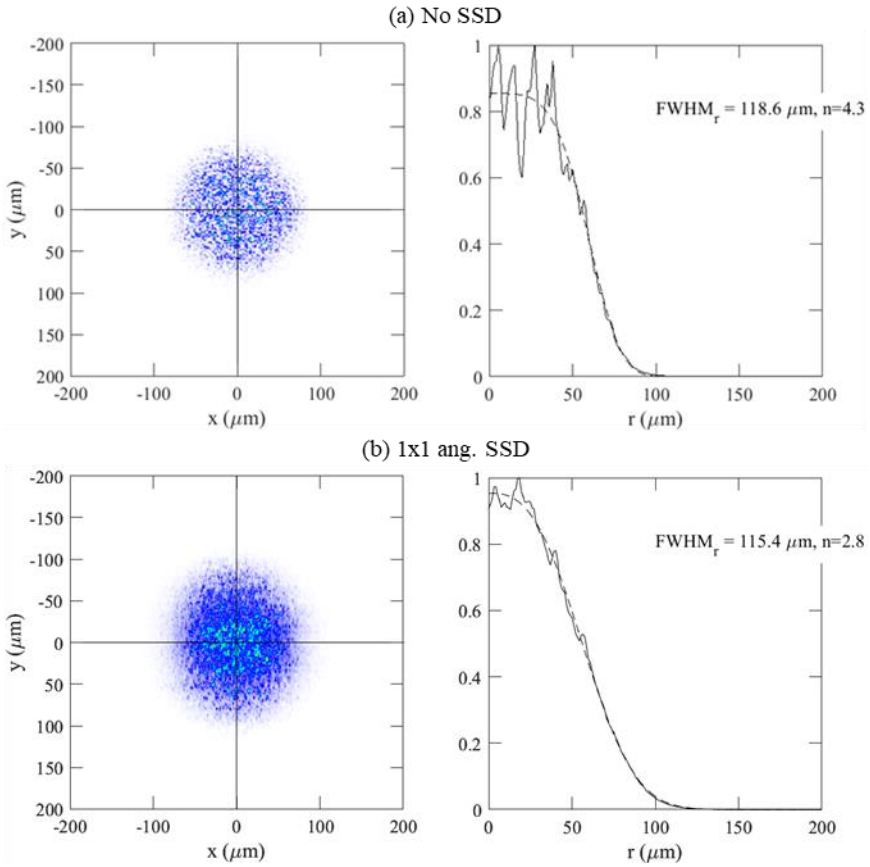

Fig. 20. Far-field P9 interaction beam profile in the gas-jet experiments (a) without SSD, or (b) with 2-D SSD with a bandwidth of 1x1 angstrom (in the infrared).

The impact of this modest level of bandwidth on the backscattering instabilities was consistent with expectations. The SRS reflectivity was not changed at all, which is consistent with SRS having growth rates that are much too high to be affected by such a modest level of bandwidth. The SBS reflectivity, on the other hand, was reduced somewhat, but this too was consistent with earlier hot-spot models of Brillouin backscatter in which the speckle motion associated with the smoothing techniques can stabilize some near-threshold speckles where the instability would take a long time to reach steady-state if stationary.

The beam spray results, however, were much more interesting. The traditional story is that the speckle motion associated with smoothing techniques can partially mitigate filamentation because the speckles move before they have sufficient time to dig density depressions in the plasma. In contrast, we observed that SSD had little to no effect on beam spray. If anything, it was aggravated, particularly in the weakly-damped nitrogen case when the filamentation figure of merit was below 1, as shown in Fig. 21. We believe this is once again related to the fact that we are in a regime where the beam spray is dominated by forward SBS. With SSD, the bandwidth is dispersed across the lens plane in such a way that different colors cross in the far field with a small difference in their pointing. Having a difference both in frequency and in wave vector, it is possible to satisfy the ion-acoustic dispersion relation, resulting in "intra-beam energy transfer" (IBET) [24] between different parts of the beam. This process drives up ion waves, and light at other frequencies can scatter off of those waves into directions outside of the incident f-cone, resulting in enhanced beam spray. We believe this is the first observation of IBET (although it has been observed in simulations) and are writing up these results for publication [25].

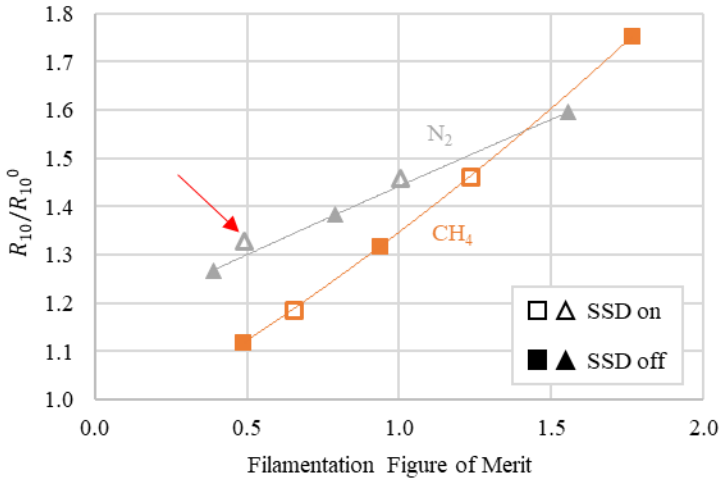

Fig. 21. New SSD-on shots plotted along with the previous SSD-off data. The SSD data were mostly in line with the previous results, but slightly exacerbated beam spray in nitrogen at the lower intensity.

Finally, the second half of the last shot day began to develop a platform with which to demonstrate that bandwidth mitigates CBET in a direct-drive implosion, as expected from simulations. Similar to the TPD platform, demonstrating CBET mitigation in an implosion-relevant configuration when only a single beam has bandwidth is not too straightforward when the effect typically involves all beams on target interacting with one another. The idea was to amplify the interaction between a specific pair of beams utilizing slightly higher-than-usual single-beam intensities and specific polarizations, and to concentrate the observable into a particular diagnostic. The baseline, narrowband case with aligned s-polarizations [Fig. 22(a)] was designed to maximize the effect of the P9 beam "pumping" a single probe beam (B25). The scattered light from B25 goes in the direction of TIM4, where it was detected by a scattered-light uniformity imager (SLUI). Figure 22(b) shows the null case using narrowband beams, where despite the lack of bandwidth the beams do not interact due to their orthogonal polarizations. The intention was to establish that those configurations give different results and then show in the future that FLUX does not pump the probe beams even when their polarizations are aligned.

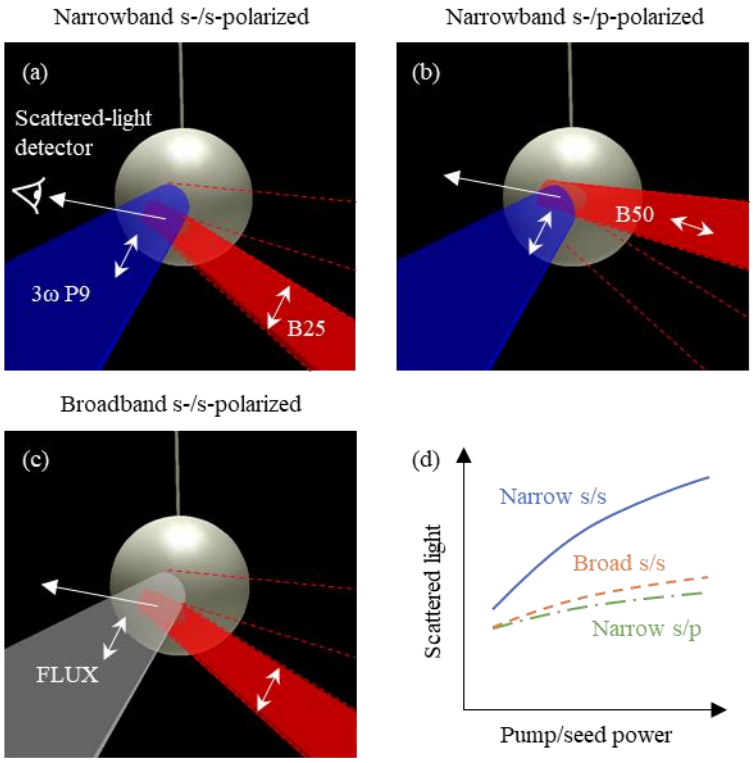

Fig. 22. A potential platform to demonstrate the effects on bandwidth on direct-drive CBET.

In practice, little difference was observed between configurations a and b on the SLUI detector. This is not fully understood but likely comes down to signal-to-noise being insufficient for detecting the diffuse scattered light from one individual beam on a spatially integrating detector that also collects scattered light from all of the other OMEGA beams. As a result, a path forward has been identified to develop a TIM-based CBET beamlets diagnostic [26] that uses spatial resolution to measure the scattered light from each individual beam separately. We believe that this will allow us to demonstrate that bandwidth mitigates CBET in direct-drive implosions, which will be one of the key deliverables from FLUX.

III. CONCLUSIONS

The novel sum-frequency-generation concept required to generate 3ω pulses with fractional bandwidth larger than 1% has been thoroughly modeled and experimentally demonstrated. This concept is being implemented on the FLUX system. The generated broadband pulses will be routed to port P9 of the Omega target chamber before focusing. Analyzing the chromaticity of the transport system, which includes an upcollimator and several diagnostic wedges has revealed the requirement to compensate for angular dispersion from diagnostic wedges and chromatic aberrations of commonly used fused-silica lenses. An angular-dispersion-compensation scheme based on two additional wedged windows has been modeled and implemented. A chromatic upcollimator based on two achromats has been designed to precompensate the chromaticity of the standard Omega fused-silica focusing lens, resulting in nearly diffraction-limited performance over a large range of wavelengths around 351 nm.

Three OMEGA shot days were executed in order to develop LPI platforms to use with FLUX in the future. A gas-jet platform will allow us to study beam spray as well as backscatter instabilities in homogenous plasmas similar to the risky regions within hohlraum interiors; excellent data were acquired for the narrowband case. A solid-target platform was tested to examine the impact of bandwidth on TPD and SRS in direct-drive implosion-relevant conditions. A prevalence of Raman backscatter and sidescatter

was observed and attributed to the high-f/# single-beam focusing geometry. Going forward, f/1 focusing capability will be developed to enable TPD studies. And finally, an attempt was made to develop an implosion-relevant platform to study the mitigation of CBET, which will be further refined in the future by upgrading the scattered-light detection to be spatially resolved in order to optimize the signal-to-noise ratio.

IV. ACKNOWLEDGMENTS

This final report summarizes the work supported by the DOE FES under Award Number DE-SC0021032. This report was prepared as an account of work sponsored by an agency of the U.S. Government. Neither the U.S. Government nor any agency thereof, nor any of their employees, makes any warranty, express or implied, or assumes any legal liability or responsibility for the accuracy, completeness, or usefulness of any information, apparatus, product, or process disclosed, or represents that its use would not infringe privately owned rights. Reference herein to any specific commercial product, process, or service by trade name, trademark, manufacturer, or otherwise does not necessarily constitute or imply its endorsement, recommendation, or favoring by the U.S. Government or any agency thereof. The views and opinions of authors expressed herein do not necessarily state or reflect those of the U.S. Government or any agency thereof.

V. REFERENCES

1. R. K. Follett, J. G. Shaw, J. F. Myatt, J. P. Palastro, R. W. Short, and D. H. Froula, "Suppressing Two-Plasmon Decay with Laser Frequency Detuning," Phys. Rev. Lett. **120**(13), 135005 (2018).
2. J. P. Palastro, J. G. Shaw, R. K. Follett, A. Colaïtis, D. Turnbull, A. V. Maximov, V. N. Goncharov, and D. H. Froula, "Resonance Absorption of a Broadband Laser Pulse," Phys. Plasmas **25**(12), 123104 (2018).
3. R. K. Follett, J. G. Shaw, J. F. Myatt, C. Dorrer, D. H. Froula, and J. P. Palastro, "Thresholds of Absolute Instabilities Driven by a Broadband Laser," Phys. Plasmas **26**(6), 062111 (2019).
4. J. W. Bates, R. K. Follett, J. G. Shaw, S. P. Obenschain, R. H. Lehmberg, J. F. Myatt, J. L. Weaver, D. M. Kehne, M. F. Wolford, M. C. Myers, and T. J. Kessler, "Suppressing Cross-Beam Energy Transfer with Broadband Lasers," High Energy Density Phys. **36**, 100772 (2020).
5. R. K. Follett, J. G. Shaw, J. F. Myatt, H. Wen, D. H. Froula, and J. P. Palastro, "Thresholds of Absolute Two-Plasmon-Decay and Stimulated Raman Scattering Instabilities Driven by Multiple Broadband Lasers," Phys. Plasmas **28**(3), 032103 (2021).
6. T. R. Boehly, D. L. Brown, R. S. Craxton, R. L. Keck, J. P. Knauer, J. H. Kelly, T. J. Kessler, S. A. Kumpan, S. J. Loucks, S. A. Letzring, F. J. Marshall, R. L. McCrory, S. F. B. Morse, W. Seka, J. M. Soures, and C. P. Verdon, "Initial Performance Results of the OMEGA Laser System," Opt. Commun. **133**(1–6), 495-506 (1997).
7. C. A. Haynam, P. J. Wegner, J. M. Auerbach, M. W. Bowers, S. N. Dixit, G. V. Erbert, G. M. Heestand, M. A. Henesian, M. R. Hermann, K. S. Jancaitis, K. R. Manes, C. D. Marshall, N. C. Mehta, J. Menapace, E. Moses, J. R. Murray, M. C. Nostrand, C. D. Orth, R. Patterson, R. A. Sacks, M. J. Shaw, M. Spaeth, S. B. Sutton, W. H. Williams, C. C. Widmayer, R. K. White, S. T. Yang, and B. M. Van Wonterghem, "National Ignition Facility Laser Performance Status," Appl. Opt. **46**(16), 3276-3303 (2007).
8. J. L. Miquel, C. Lion, and P. Vivini, "The Laser Mega-Joule: LMJ & PETAL status and Program Overview," J. Phys.: Conf. Ser. **688**, 012067 (2016).
9. C. Dorrer, E. M. Hill, and J. D. Zuegel, "High-Energy Parametric Amplification of Spectrally Incoherent Broadband Pulses," Opt. Express **28**(1), 451-471 (2020).
10. C. Dorrer, "Optical Parametric Amplification of Spectrally Incoherent Pulses," J. Opt. Soc. Am. B **38**(3), 792-804 (2021).

11. N. Ekanayake, M. Spilatro, A. Bolognesi, S. Herman, S. Sampat, E. M. Hill, and C. Dorrer, "Design and Optimization of a High-Energy Optical Parametric Amplifier for Broadband, Spectrally Incoherent Pulses," Opt. Express **31**(11), 17848–17860 (2023).
12. C. Dorrer, M. Spilatro, S. Herman, T. Borger, and E. M. Hill, "Broadband Sum-Frequency Generation of Spectrally Incoherent Pulses," Opt. Express **29**(11), 16135-16152 (2021).
13. D. Eimerl, E. M. Campbell, W. F. Krupke, J. Zweiback, W. L. Kruer, J. Marozas, J. Zuegel, J. Myatt, J. Kelly, D. Froula, and R. L. McCrory, "StarDriver: A Flexible Laser Driver for Inertial Confinement Fusion and High Energy Density Physics," J. Fusion Energ. **33**(5), 476-488 (2014).
14. N. Fleurot, C. Cavailler, and J. L. Bourgade, "The Laser Mégajoule (LMJ) Project Dedicated to Inertial Confinement Fusion: Development and Construction Status," Fusion Eng. Des. **74**(1–4), 147-154 (2005).
15. David Turnbull, Arnaud Colaïtis, Aaron M. Hansen, Avram L. Milder, John P. Palastro, Joseph Katz, Christophe Dorrer, Brian E. Kruschwitz, David J. Strozzi, and Dustin H. Froula, "Impact of the Langdon effect on crossed-beam energy transfer," Nature Physics **16**(2), 181-185 (2020).
16. J. Sheffield, D. Froula, S. H. Glenzer, and N. C. Luhmann, Jr., *Plasma Scattering of Electromagnetic Radiation: Theory and Measurement Techniques*, 2nd ed. (Academic Press, New York, 2010).
17. R. S. Craxton, "High Efficiency Frequency Tripling Schemes for High Power Nd:Glass Lasers," IEEE J. Quantum Electron. **QE-17**(9), 1771-1782 (1981).
18. M. D. Skeldon, R. S. Craxton, T. J. Kessler, W. Seka, R. W. Short, S. Skupsky, and J. M. Soures, "Efficient Harmonic Generation with a Broad-Band Laser," IEEE J. Quantum Electron. **28**(5), 1389-1399 (1992).
19. C. Dorrer and M. Spilatro, "Spectral and Temporal Shaping of Spectrally Incoherent Pulses in the Infrared And Ultraviolet," Opt. Express **30**(4), 4942-4953 (2022).
20. C. Dorrer, "Analysis of the Nonlinear Propagation of Incoherent Pulses," Opt. Express **31**(5), 7789–7806 (2023).
21. V. I. Bespalov and V. I. Talanov, "Filamentary Structure of Light Beams in Nonlinear Liquids," JETP Lett. **3**(12), 307-310 (1966).
22. M. Grech, G. Riazuelo, D. Pesme, S. Weber, and V. T. Tikhonchuk, "Coherent Forward Stimulated-Brillouin Scattering of a Spatially Incoherent Laser Beam in a Plasma and Its Effect on Beam Spray," Phys. Rev. Lett. **102**(15), 155001 (2009).
23. D. Turnbull, J. Katz, D. E. Hinkel, P. Michel, R. L. Berger, T. Chapman, L. Divol, C. Dorrer, E. Kur, S. MacLaren, A. V. Milder, M. Rosen, A. Shvydky, and D. H. Froula, "Beam-Spray Thresholds in Inertial Confinement Fusion-Relevant Plasmas," Phys. Rev. Lett. **129**(2), 025001 (2022).
24. P. M. Michel J. D. Ludwig, T. Chapman, and M. Belyaev, in review
25. J. Katz D. Turnbull, T. Chapman, J. Ludwig, P. Michel, and D. H. Froul, in preparation for Physics of Plasmas
26. D. H. Edgell, A. M. Hansen, J. Katz, D. Turnbull, and D. H. Froula, "Unabsorbed Light Beamlets for Diagnosing Coronal Density Profiles and Absorption Nonuniformity in Direct-Drive Implosions on OMEGA," Rev. Sci. Instrum. **92**(4), 043525 (2021).